Soft Matter

Ionic strength and molecular weight effects on floc formation and growth in Taylor-Couette flows

Journal:	*Soft Matter*
Manuscript ID	SM-ART-08-2020-001517.R1
Article Type:	Paper
Date Submitted by the Author:	02-Nov-2020
Complete List of Authors:	Metaxas, Athena; University of Minnesota, Department of Chemical Engineering and Materials Science Panwar, Vishal; University of Minnesota, Department of Mechanical Engineering Olson, Ruth; Northwestern University, Chemical and Biological Engineering; University of Minnesota, Department of Mechanical Engineering Dutcher, Cari; University of Minnesota, Department of Mechanical Engineering; University of Minnesota Twin Cities, Chemical Engineering and Materials Science

Ionic strength and molecular weight effects on floc formation and growth in Taylor-Couette flows

*Athena E. Metaxas,[1] Vishal Panwar,[2] Ruth L. Olson,[3] and Cari S. Dutcher[1,2,] **

[1] Department of Chemical Engineering and Materials Science, University of Minnesota – Twin Cities, 421 Washington Ave SE, Minneapolis, MN 55455, USA

[2] Department of Mechanical Engineering, University of Minnesota - Twin Cities, 111 Church Street SE, Minneapolis, MN 55455, USA

[3] Department of Chemical and Biological Engineering, Northwestern University, 2145 Sheridan Road, Evanston, IL 60208, USA

*Corresponding Author Email: cdutcher@umn.edu

Keywords: flocculation, Taylor-Couette flows, aqueous colloidal suspensions, mixing, radial fluid injection, bentonite, polyelectrolytes

Abstract

Polyelectrolyte-driven flocculation of suspended particulate in solution is an important process in a variety of industrial processes such as drinking water treatment and composite material synthesis. Flocculation depends on a wide variety of physicochemical and hydrodynamic properties, which affects floc size, growth rate, and morphology. Floc formation and growth behavior is explored here using two different molecular weights of a cationic polyacrylamide flocculant and anisotropic Na-bentonite clay particles under a variety of solution ionic strengths. A Taylor-Couette cell with radial injection capabilities was used to study the effects of solution ionic strength and polyelectrolyte molecular weight on floc size, growth rate, and morphology during the flocculation process with a constant global velocity gradient. The floc size generally decreased with increasing ionic strength whereas the floc growth rate initially increased then decreased. This likely occurred due to charge screening effects, where increased bentonite aggregate size and a less expanded polyelectrolyte conformation at higher ionic strengths results in a decreased ability for the polyelectrolyte to bridge multiple bentonite aggregates. The densification of bentonite aggregates at higher ionic strengths resulted in floc morphologies that were more resistant to shear-induced breakage. With the exceptions of optimal dose concentration and dispersion coefficients, there were no clear differences in the floc growth rate behaviors for the two molecular weights studied. This work contributes to an improved understanding of the physicochemical complexities of polyelectrolyte-driven flocculation that can inform dosing requirements for more efficient industrial operations.

Introduction

Polyelectrolytes, or polymers with charged functional groups, are used in a variety of applications such as drag reduction, enhanced oil recovery, paper manufacturing, and flocculation in drinking water treatment.[1–5] In flocculation, polyelectrolytes are added to a particulate-laden suspension so that they adsorb to multiple suspended particulates, forming structures known as flocs that can be readily separated from solution. Rapid floc growth occurs during mixing by orthokinetic aggregation, where the particulates with adsorbed polyelectrolyte collide and grow due to the shear gradients present in the flow.[6–8] The variation in chemical composition of the aqueous solutions along with the complexity of the hydrodynamics involved in mixing make understanding the process of flocculation difficult to understand. This results in reliance of highly empirical methods to determine polyelectrolyte flocculant dosing amounts in applications like drinking water treatment.

The particulate of interest in this study is bentonite, a clay particle commonly found in surface waters that has been used in prior flocculation studies.[9–12] Bentonite itself is an aggregate of many thin sheets, where the basal planes consist of permanent negative charges, and the edges consist of hydroxyl groups where the charge can vary with pH.[13,14] Due to these surface charges, the morphology of the bentonite aggregate is susceptible to changes in solution ionic strength or pH. An increase in solution ionic strength results in a change in the bentonite structure from a more porous morphology to a denser morphology. This change in aggregate structure has been indirectly confirmed with rheological measurements and confocal microscopy and directly confirmed with scanning electron microscopy.[15–22] Changes in solution ionic strength also have consequences for bentonite aggregate size. A previous study by Wilkinson et al.[21] showed that an

increase in solution ionic strength resulted in an increase by two orders of magnitude of the initial bentonite aggregate size, which is attributed to the decrease in Debye length between bentonite sheets. This allows aggregation of the bentonite sheets to form denser, face-face morphologies and larger bentonite aggregates in solution.[7,23]

The variations in bentonite aggregate surface morphology and aggregate size due to changes in solution ionic strength result in different adsorption capacities and interaction potentials with the polyelectrolyte flocculant that is added to a bentonite-laden suspension, thus increasing the complexity of fundamentally understanding flocculation.[24] In addition to charge screening affecting the aggregate structure of the bentonite, the polyelectrolyte present in solution will also change conformation depending on the ionic strength of the solution. At lower ionic strengths, the charged moieties along the polymer backbone are not sufficiently screened, and the polymer chains adopt an expanded conformation, resulting in larger persistence lengths. At higher ionic strengths, the charged moieties are now screened, and the polymer chains adopt a coil-like conformation, resulting in smaller persistence lengths.[3,25,26]

The mixing environmental also influences the flocculation behavior. One method to test for flocculation performance is with jar tests, which replicate scaled-down industrial mixing tanks for flocculation. Jar tests are a relatively rapid, easy technique to obtain a lot of information about flocculation processes, but they lack homogeneous spatial and temporal flow features and possess un-controlled shear stresses, thus making it difficult to attribute certain floc properties to a specific flow features.[27,28] Instead, Taylor-Couette (TC) cells, which consists of two concentric cylinders with a specified gap width, can be used as they can generate a controlled variety of laminar and turbulent flow states as a function of cylinder speed.[18,29–33] Prior flocculation studies using a TC cell were limited in that the flocs had to be pre-formed outside of the cell.[34–36] A TC

cell with a glass outer cylinder for imaging and an inner cylinder modified for radial injection was recently constructed to directly inject the polymer flocculant into the annulus, so that the full flocculation process can be studied in-situ.[37,38] This unique TC cell was used previously by the authors in Metaxas et al.[39] to test the effects of initial mixing speed, which corresponds to a specific vortex type in the TC cell, on the flocculation of bentonite with a cationic polyacrylamide flocculant. It was found that an increase in the early mixing speed results in an increased floc growth rate, but the maximum floc sizes were similar in size.

While *in-situ* bentonite-polyelectrolyte flocculation work by Metaxas et al.[39] enabled a first study of flocculation in varying TC flows, the influence of changes in solution chemical composition was not examined as the ionic strength of the suspension, the polyelectrolyte molecular weight, and the concentration of polyelectrolyte were constant. However, the known ionic strength-dependence of size and morphology of the bentonite aggregate as well as the ionic strength-dependence of polyelectrolyte persistence length and conformation adds an important additional complexity to understanding flocculation dynamics. The ionic strength-induced changes in polyelectrolyte chain conformation will modify the extent that extensional forces present in the flow field around the polymer act to stretch the polyelectrolyte chains and enhance the bridging capability of the polyelectrolyte.[40,41] In this work, we vary ionic strength and molecular weight to understand the effects of these properties on the flocculation process, specifically the floc size, floc growth rate, and floc morphology, in well-controlled flow conditions.

1 Materials and Methods

118 1.1 Materials

119 The polymer flocculants, or organic polyelectrolytes, used in this study are both
120 commercially available cationic polyacrylamides (FLOPAM FO 4190SH and FLOPAM FO
121 4190SSH, SNF Polydyne) with 10 mol% of the monomer groups containing a quaternary
122 ammonium cation with a permanent positive charge in solution. The FLOPAM 4190SH has a
123 molecular weight of 4-6 x 10^6 g·mol^{-1} and the FLOPAM 4190SSH has a molecular weight of 8-
124 11 x 10^6 g·mol^{-1}. For both cationic polyacrylamides (CPAM), a 0.2 wt% solution was made by
125 mixing the solid polymer pellets with a Jiffy mixer attachment in distilled water for 30 min. The
126 solutions rested in a refrigerator overnight prior to use and were remade every 2 weeks as
127 necessary as indicated by the supplier. Before any experiment was performed, the solution was
128 removed from the refrigerator and allowed to warm to room temperature (~23°C). The distilled
129 water was purchased from Premium Waters, Inc. Powdered Na-Bentonite and NaCl are ACS
130 grade from Fisher Scientific and were used as received.

131 1.2 Methods: Jar Tests

132 To perform a jar test, the appropriate amount of NaCl needed to obtain ionic strengths,
133 [I], of 0 mM (no NaCl), 1.3 mM, 10 mM, and 100 mM was added to 1 L of distilled water in a 2
134 L Pyrex beaker, or jar. A VELP Scientifica JTL4 flocculator was used to mix the solutions for 5
135 min at 300 RPM to fully dissolve the NaCl. The bentonite was then added to the jar to mix for 30
136 min at 300 RPM to evenly distribute it. For all jar tests, the concentration of bentonite was kept
137 constant at 30 mg·L^{-1}. The mixing speed was then lowered to 200 RPM, and a pre-specified
138 volume of polyelectrolyte flocculant was injected into the suspension and mixed for 3 min to
139 disperse the flocculant. To allow the flocs to grow, the mixing speed was lowered to 30 RPM
140 and the suspension was mixed for an additional 30 min. Once the mixing stopped, the jars sat for
141 5 min before the final turbidity in nephelometric turbidity units (NTU) was measured with a

LaMotte turbidity meter. This was performed for a range of polyelectrolyte flocculant concentrations in triplicate at each concentration to obtain the optimal dose, which is the global minimum in a turbidity curve as shown in Figure 1. The optimal dose for each ionic strength and polyelectrolyte type is shown in Table 1. The steady shear viscosities of each suspension with the optimal dose of polyelectrolyte were measured using the cup and bob geometry fixture of an AR-G2 rotational rheometer from 1 s^{-1} to 250 s^{-1} at 23°C as shown in Figure S1 and were found to be Newtonian for the range of shear rates experienced in the annulus of the TC cell.

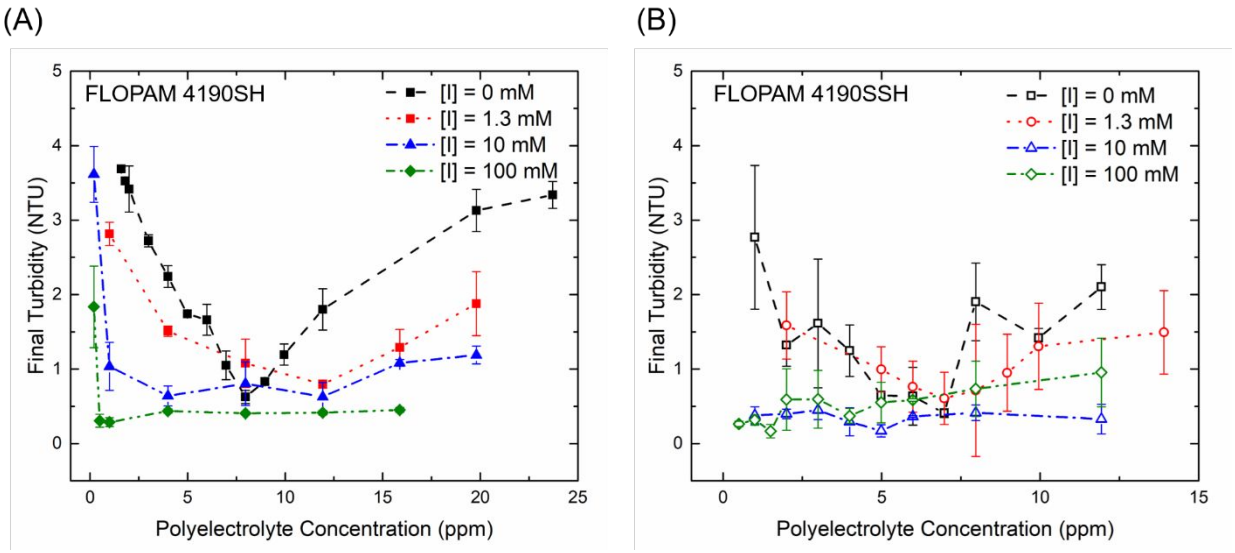

Figure 1: Jar test results as a function of solution ionic strength using the (A) lower molecular weight cationic polyacrylamide flocculant (4190SH) and the (B) higher molecular weight cationic polyacrylamide flocculant (4190SSH). The final turbidity in terms of nephelometric turbidity units (NTU) is expressed as a function of the polyelectrolyte dose, or concentration, in parts per million (ppm). The global minimum in each curve denotes the optimal dose for a set of solution conditions. Error bars represent one standard deviation from the mean turbidity.

1.3 Methods: Suspension Loading into TC Cell Annulus and Spatial Calibration

The TC cell used in this study injects flocculant through a total of 16 precisely spaced axial and azimuthal injection ports along the inner cylinder to smooth any azimuthal concentration gradients. These injection ports do not protrude into the annulus and the port covers are contour-matched to the inner cylinder so that the flow profile of the resultant vortices

are not modified during operation.[38] Additional details on the TC cell design, with inner cylinder diameter ($D_i = 2R_i$) of 13.5407 ± 0.0025 cm, gap width (d) of 0.84 cm, and the injection assembly can be found elsewhere.[37] To make the bentonite suspensions, the appropriate amount of NaCl was added to two separate 2 L jars each filled with 1 L distilled water to obtain solutions with ionic strengths of 0 mM (no NaCl), 1.3 mM, 10 mM, or 100 mM. The NaCl was mixed using a VELP Scientifica JTL4 Flocculator for 5 min at 300 RPM. Once the NaCl was dissolved, 30 mg of bentonite was transferred to each jar to have a total of 2 L of 30 $mg \cdot L^{-1}$ bentonite suspensions. The bentonite was dispersed using the flocculator for 30 min at 300 RPM. The pH of the suspensions in all cases was approximately 6.6 due to the interaction of dissolved carbon dioxide in water and bentonite.[42] Once finished, the bentonite suspensions were immediately transferred to the annulus of the TC cell by way of tubing attached to the base of the cylinder assembly. A figure detailing this process can be found in a previous study by Metaxas et al.[39]

1.4 Methods: Flocculation Experiment Protocol

A stepper motor (Applied Motion Products HT34-497 2 phase stepper motor with a STAC5-S-E120 controller) rotates the inner cylinder and is equipped with a 7:1 gear reducer (Applied Motion Products 34VL007) for inertial balance between the motor and the cylinder. A laser diode (Thorlabs, 450 nm, 1600 mW max) in combination with a laser line generator was used to create a laser light sheet tangential to the inner cylinder. The Basler Ace camera (1280 × 1024 pixels, 60 fps maximum frame rate) with a Tamron 25 mm c-mount lens was vertically adjusted such that the field of view was between the third and fourth injection port covers from the bottom of the TC cell. The frame rate on the camera was set to 30 fps with an exposure time of 8 ms for all experiments. A LabView code was used to simultaneously inject the polyelectrolyte flocculant from the inner cylinder ports into the annulus and record the entire

flocculation process. For all experiments, the drive pressure was set to 30 psi to inject the 0.2 wt% polyelectrolyte solution at a calibrated injection rate of 1.115 ± 0.089 $g \cdot s^{-1}$ for the 4190SH flocculant and 0.772 ± 0.039 $g \cdot s^{-1}$ for the 4190SSH flocculant. The calibration data can be found in the Supplementary Information (Figure S2). The injection time was based on the required mass of flocculant needed to obtain the concentrations shown in Table 1.

Many flocculation applications preform the mixing with a two-stage protocol. First, there is an initial faster "Mix" speed (Stage 1), followed by a slower "Growth" speed (Stage 2), although growth can occur during both Stage 1 and Stage 2. In this study, the Mix and Growth speeds were set to constant rotation speeds of 0.50 s^{-1} and 0.46 s^{-1}, respectively. To begin an experiment, the inner cylinder drive shaft and injection ports were primed with flocculant. The initial Stage 1 speed was set, and the recording was started. After a delay of 30 s, the polymer was injected from the inner cylinder into the annulus and mixed at this Stage 1 speed for 3 min. After this, a step change in speed occurred to reach the Stage 2. This stage was maintained for 30 min to allow the flocs to grow. The speed of 0.46 s^{-1} was chosen as it was the slowest speed tested that allowed flocs to be suspended throughout the 30 min duration of Stage 2 mixing. The times (3 min for Stage 1 and 30 for min Stage 2) used here mimic those used in the jar tests described in Section 2.2. After completion, the TC cell was disassembled and cleaned.

1.5 Methods: Image Analysis

Physicochemical and hydrodynamic effects on final floc microstructure have been examined using techniques such as small angle light scattering, which yields final floc size and fractal dimensions.[43–45] The longer characterization length scales accessible by static light scattering typically work well to determine mass fractal dimension determination. However, interpretation of the scattering patterns can be difficult, and static light scattering works best for

small aggregates with loosely packed structures, which is not always the case during flocculation. In more recent years, advanced image analysis techniques have been used to study the dynamic flocculation behavior using jar tests and impellers. Image analysis offers a non-intrusive method of studying the flocs as compared to obtaining and preparing a sample for light scattering experiments.[46]

To eliminate the curved glass surface of the outer cylinder during imaging, refractive index-matching paraffin oil was poured into the Plexiglass tank surrounding the TC cell prior to making the bentonite suspension. The cell was illuminated using a flicker-free LED light strip (Metaphase 19 in Exo2 Light) to visualize the bottom-most port cover of the inner cylinder. An image of the port cover was captured with the Basler camera. ImageJ was then used to determine the pixel-to-mm ratio of the port cover for spatial calibration of the flocculation movies.

The movies were post-processed using MATLAB to obtain time-dependent floc size and morphology based on an analysis by Vlieghe et al.[47] The raw movie frames were first binarized to clearly show the floc (shown as white shapes in Figure 2 and Figure S3), and the centroid position of each floc (x_c,y_c) was determined. As a metric of floc size, the radius of gyration, R_g, of the non-spherical floc is calculated via

$$R_g^2 = \frac{1}{N_p}\sum_{i=1}^{N_p}\left[(x_i - x_c)^2 + (y_i - y_c)^2\right] \#(1)$$

where N_p is the number of pixels making up each floc with coordinate pair (x_i, y_i). The resulting radii of gyration were averaged for each 10 s interval (300 frames).

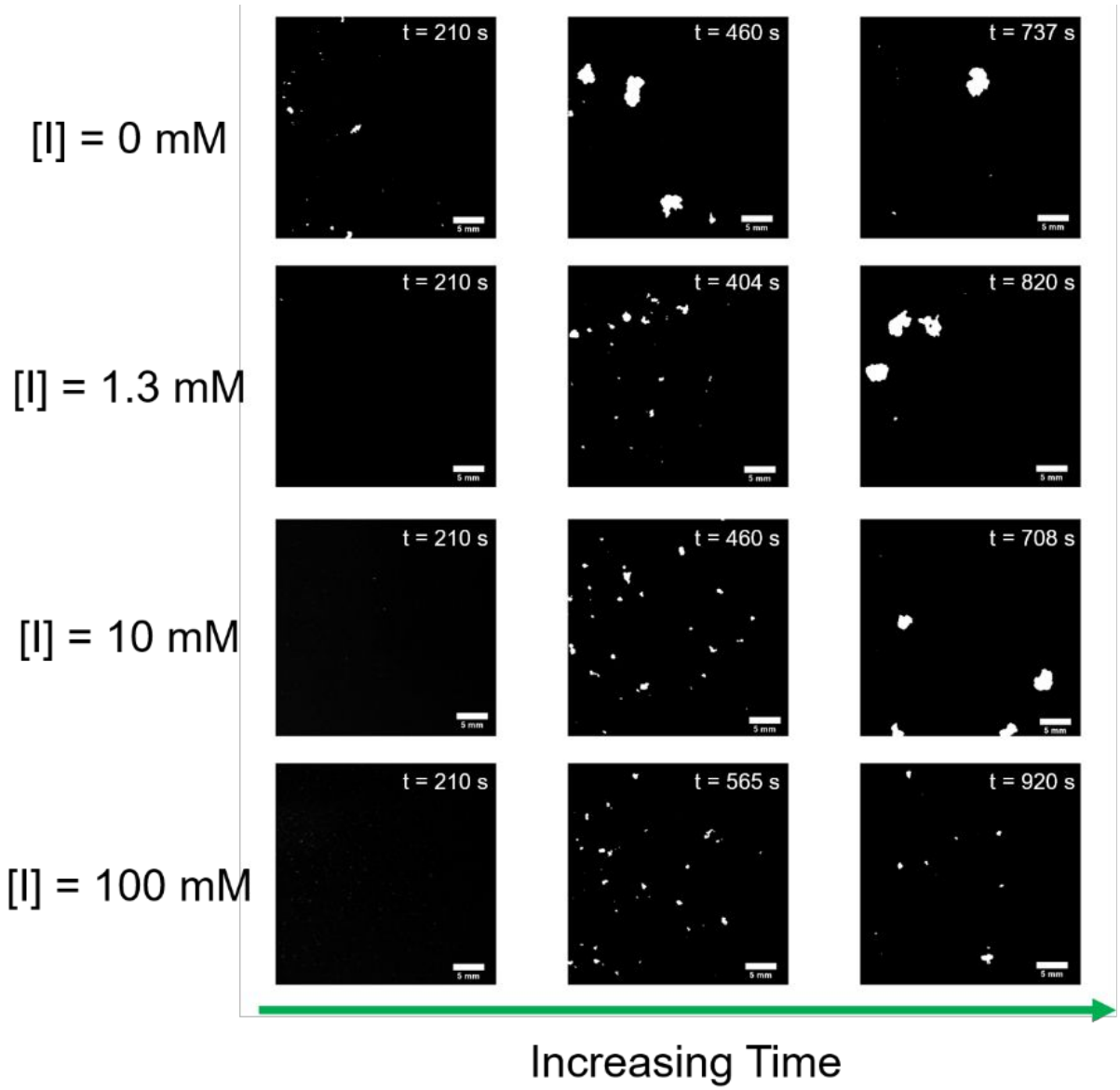

Figure 2: Time lapse of binarized images of bentonite-cationic polyacrylamide flocs (here, the 4190SH flocculant was used) as a function of ionic strength. The first image in each row is at 210 s, which is the onset of the inner cylinder speed change from Stage 1 to Stage 2 mixing. The last image in each row occurs where the floc size plateaus. The middle image in each row occurs at the midpoint time between the times associated with the first and last images. The white scale bar in the lower right-hand corner of each image represents 5 mm. The movie frames have been resized to comply with figure dimension limitations. The actual movie frames used in the quantitative analysis are larger than what is shown here (actual dimensions of each frame are 1280 × 1024 pixels).

A 2-D surface-based fractal dimension, D_{sf}, was used to quantify the morphology of the flocs. This quantity was calculated using the cross-sectional floc area, A, and the floc perimeter, P, using the relationship from Vlieghe et al.[47]

$$A \propto P^{2/D_{sf}} \#(2)$$

The fractal dimension varies between the limits of 1, which indicates a circular floc cross-section, and 2, which indicates a rod-like floc cross-section. For each 10 s set of data, a linear regression was performed to determine D_{sf}. The number of flocs as a function of time were also calculated for each experiment. All experiments were conducted in triplicate for error analysis. All runs for both the 4190SH and 4190SSH flocculants are shown in Figures S4 and S5, respectively.

2 Results and Discussion

2.1 Optimal Dose Determination of Polyelectrolyte Flocculants

Jar tests were performed to determine the optimal dose of polyelectrolyte required as a function of both the solution ionic strength and the polyelectrolyte type. The optimal dose occurs where there is a global minimum in the turbidity curve. Determining the optimal dose is critical because under-dosing results in insufficient particulate removal and over-dosing results in particulate restabilization, both undesirable outcomes which can be cost-prohibitive in water treatment.[48–50] As discussed earlier, Figure 1 shows the results from these jar tests for both the lower molecular weight (4190SH) and higher molecular weight (4190SSH) cationic polyacrylamides. The optimal dose decreases as the ionic strength increases for both polyelectrolytes as reported in Table 1. The global minimum in the final turbidity indicates that more solid particulate (in this the case, bentonite) has settled out of solution because of the

presence of the flocculant and the increase in ionic strength of the solution. The shape of the turbidity curves also differs with ionic strength, where there is a distinct minimum in the curve below [I] = 10 mM and a loss of the distinct minimum at [I] = 10 mM and above. This suggests the restabilization of bentonite due to overdosing as previously mentioned.

The previously mentioned study by Wilkinson et al.[21] showed that an increase in solution ionic strength resulted in an increase in the bentonite aggregate size from ~0.04 μm at [I] = 0 mM to ~9 μm at [I] = 100 mM, which is attributed to the decrease in Debye length between bentonite sheets. In brief, the net negative charge of the bentonite platelets is screened by an increase in positive Na^+ ions added as NaCl into solution, which decreases the repulsive, electrostatic force between the bentonite platelets, allowing them to aggregate to form larger bentonite aggregates.[7,23] Aggregation of the bentonite clay is aided just by the presence of additional NaCl in the solution, which means less of the polyelectrolyte is required to promote flocculation efficiency. The optimal doses of the higher molecular weight CPAM at each solution ionic strength were generally lower than those of the lower molecular weight CPAM. Because both polyelectrolytes in the study consist of the same monomer unit, the higher molecular weight polyelectrolyte is longer in length and therefore able to bridge more bentonite aggregates, requiring less of the polymer in solution to produce similar flocculation efficiencies.[1,51]

2.2 Ionic Strength and Molecular Weight Effects on Floc Size and Growth Rate

Once the optimal doses were determined for each polyelectrolyte at every solution ionic strength and the TC cell was calibrated to inject the correct mass of polyelectrolyte (see Figure S2), the flocculation experiments were conducted in the TC cell with radial injection capabilities. As described in the Methods section, during a routine flocculation processes, the flocculant is

first rapidly mixed (Stage 1) to disperse the polymer quickly, followed by a slower mix (Stage 2) to allow appreciable floc growth.[52] For this study, the inner cylinder rotational speed, $\Omega_{i,}$, for Stage 1 and Stage 2 mixing were both kept constant at 0.50 s^{-1} and 0.46 s^{-1}, respectively.

While Ω_i remained constant for both the Stage 1 and Stage 2 mixing, there is some variation in the non-dimensionalized velocity, given by the Reynolds number ($Re_i = \Omega_i R_i d/\nu$), due to slight differences in the kinematic viscosity ν of each suspension. The Stage 1 Re_i range from 1517, 1518, 1956, and 1785 for the lower molecular weight CPAM and from 1593, 1822, 1792, and 1709 for the higher molecular weight CPAM as ionic strength increases. The Stage 2 Re_i range from 1404, 1405, 1810, and 1654 for the lower molecular weight CPAM and from 1474, 1687, 1659, and 1582 for the higher molecular weight CPAM as ionic strength increases. Even though the Re_i vary, they all fall within the range for the turbulent wavy vortex (TWV) flow type, which the Re_i range for TWV flow for this specific TC geometry falls between 1400 and 2924. The prior TC flocculation study by Metaxas et al.[39] tested two different Re_i within a vortex flow type and found no statistical difference in the floc size, growth rate, and floc morphology, therefore it can be assumed that the same holds true in this study.

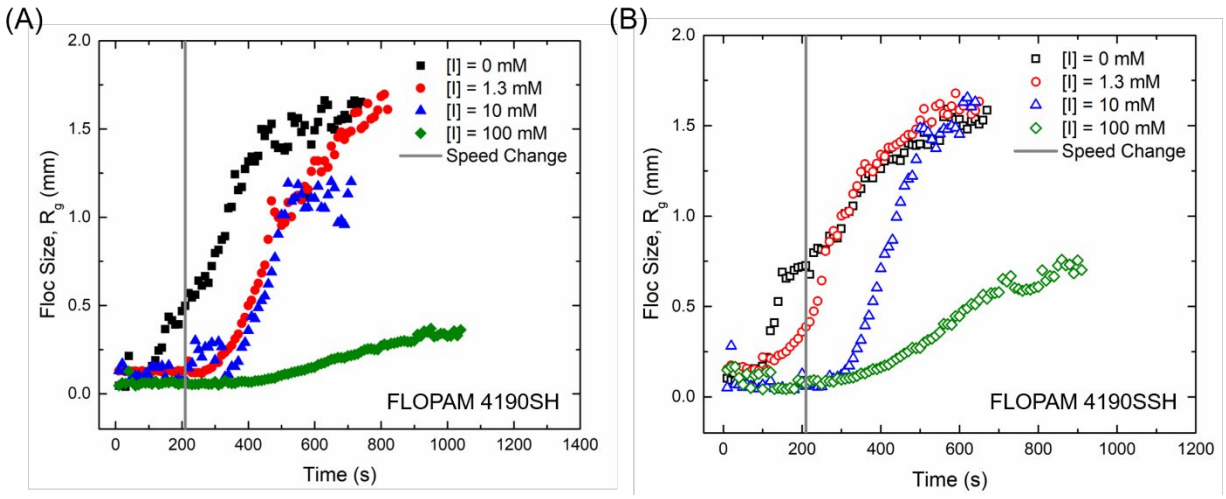

Figure 3: Floc size expressed as radius of gyration, R_g, as a function of ionic strength with time for the (A) lower molecular weight cationic polyacrylamide flocculant (4190SH) and the (B) higher molecular weight cationic polyacrylamide flocculant (4190SSH). The vertical gray line depicts where the inner cylinder speed transitions from $\Omega_i = 0.5$ s^{-1} to $\Omega_i = 0.46$ s^{-1}.

Figure 3 depicts a representative example of the transient floc size, expressed as the radius of gyration R_g, as a function of solution ionic strength and polyelectrolyte molecular weight. The radius of gyration of the flocs increases in all runs after the initial injection of cationic polyacrylamide at 30 seconds until a plateau value of R_g is obtained. Shear gradients present in the flow and a finite amount of bentonite and flocculant limit the maximum floc size.[8,34,46,53] The maximum floc size generally decreases as ionic strength increases, from 1.8 ± 0.3 mm at [I] = 0 mM to 0.4 ± 0.1 mm at [I] = 100 mM for the lower molecular weight CPAM (4190SH) and from 1.9 ± 0.2 mm at [I] = 0 mM to 0.6 ± 0.3 mm at [I] = 100 mM for the higher molecular weight CPAM (4190SSH) as shown in Table 1. The floc sizes tend to be slightly larger for the 4190SSH CPAM compared to the 4190SH CPAM as the 4190SSH variant is higher in molecular weight and therefore is longer in length, allowing it to bridge more bentonite aggregates.[1,11,51] All experimental runs can be found in the SI (Figures S4 and S5).

The floc growth rate can be calculated from the experimental data using a modified version of the logistic growth equation

$$\frac{R_g(t)}{R_{g,\,max}} = \frac{1}{1 + \left(\frac{1}{R_{g,\,0}/R_{g,max}} - 1\right)e^{-rt}} \#(3)$$

where R_g is the radius of gyration at a given time in mm, $R_{g,max}$ is the maximum value of R_g in the fitting range in mm, $R_{g,0}$ is the initial value of R_g at the beginning of the fitting range in mm, r is the growth rate in mm s^{-1}, and t is time in seconds. This model is typically used for quantifying growth rates in microbial and ecological studies, but it can also be applied to quantify floc growth rates as the flocs eventually plateau in growth due to finite concentrations of bentonite and polyelectrolyte, which is akin to a "carrying capacity."[39,54–56] The logistic growth equation was fit to where there was a marked increase in the floc size with time. An example of the logistic growth fit is shown in Figure 4, and all fits are shown in Figures S6-S7. In addition to the fits, the residuals between the measured values and calculated values from the modified logistic growth equation are presented to show how well the logistic growth equation fits the data points.

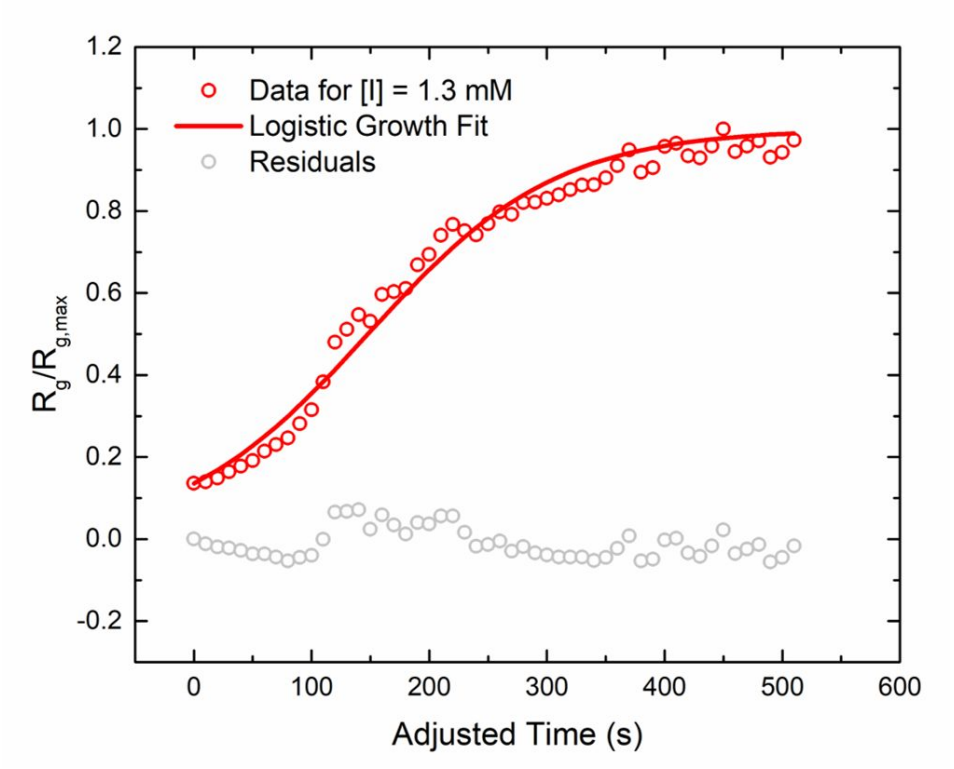

Figure 4: Representative example of the logistic growth fit to floc size data over time using the higher molecular weight polyelectrolyte (4190SSH) at a solution ionic strength of [I] = 1.3 mM. The open, red circles represent the R_g data points collected during the experiment normalized by the maximum value of R_g in the fitting range, which is where the floc size plateaus. The solid, red line indicates the logistic growth fit. The open, gray circles represent the residuals of the fit, which is the data point calculated using the logistic growth model subtracted from the original data at each corresponding time point. The time was adjusted such that the beginning of floc growth occurs at time = 0 s. Logistic growth fits for all systems can be found in Figures S6-S7.

For both polyelectrolytes tested in this study, the floc growth rate initially increases from 0.010 ± 0.002 mm s^{-1} for 4190SH and 0.008 ± 0.004 mm s^{-1} for 4190SSH at [I] = 0 mM to 0.020 ± 0.003 mm s^{-1} for 4190SH and 0.020 ± 0.002 mm s^{-1} for 4190SSH at [I] = 10 mM as shown in Table 1. Once the solution ionic strength is increased to [I] = 100 mM, the growth rates decrease to 0.008 ± 0.005 mm s^{-1} for 4190SH and 0.009 ± 0.005 mm s^{-1} for 4190SSH. This initial increase in growth rate followed by a decrease as the solution ionic strength increases is due to the interplay of two factors: (1) the bentonite aggregate size increases with ionic strength and (2) the persistence length, and therefore how stretched out the polyelectrolyte conformation is in

solution, decreases.[3,21] In particular, the change in persistence length of the polyelectrolytes affects how effectively the polyelectrolyte bridges multiple bentonite aggregates. When there are no or very few additional ions in solution (i.e. [I] = 0 mM and [I] = 1.3 mM), the positive charges of the quaternary ammonium cation functional groups on the polyelectrolyte backbone repulse each other, forcing the polyelectrolyte to adopt a more rigid, expanded conformation with a larger persistence length compared to those at higher ionic strengths.[3,25,57]

Similarly to the bentonite sheets and aggregates, as the solution ionic strength increases ([I] = 10 mM and [I] = 100 mM), the positive charges of the quaternary ammonium functional groups on the polymer backbone are increasingly screened due to an increase in negative Cl^- ions present in solution. This then allows for the polyelectrolyte to adopt a more flexible, coiled conformation and the persistence length therefore decreases.[3,25] Walldal and Åkerman[25] found that for the same CPAM with a molecular weight in the same range as the ones used in this study (5×10^6 g·mol^{-1}), the persistence length decreased from ~8.5 nm at [I] = 0 mM to ~5.5 nm at [I] = 10 mM until it finally plateaued to ~2 nm at [I] = 45 mM. The [I] = 10 mM appears to be an inflection point as at that point the bentonite aggregates prior to the addition of CPAM are two orders of magnitude larger than those at [I] = 0 mM as shown by Wilkinson et al.,[21] but the persistence lengths of the polyelectrolytes are not so small that the bridging capability of the CPAM is significantly decreased, which could explain why the growth rate has increased and why there is a delay in the growth at [I] = 100 mM compared to the other ionic strengths tested. At [I] = 100 mM, the bentonite aggregate size prior to the addition of CPAM is another order of magnitude larger than that at [I] = 10 mM, but the persistence lengths of the polyelectrolytes have continued to decrease, and the polymer chains cannot bridge the now much larger bentonite aggregates as effectively, leading to smaller floc sizes and growth rates. The images in Figure 2

and Figure S3 illustrate this point as the flocs are visibly larger at the lower ionic strengths and smaller at the higher ionic strengths.

As the flocs are formed and grow during the flocculation process, they can eventually break due to fluid shear forces.[46,47] After some time, the flocs will approach a steady state between floc growth and breakage.[58–61] Prior studies have shown that the maximum floc size is on the order of the Kolmogorov microscale, and floc size decreases with increasing global velocity gradient via the global dissipation rate of turbulent kinetic energy.[34,39,46,62] However, the global velocity gradient in this study does not significantly vary, if at all, because the kinematic viscosities of the suspensions are quite similar to each other (~1 cSt to ~1.2 cSt) and the same inner cylinder speed and vortex flow type were used in all experiments. Here, the global velocity gradient, $G \approx 2\pi R_i \Omega_i / d$, is 25.1 s^{-1} for Stage 1 mixing for 3 min and 23.3 s^{-1} for Stage 2 mixing for 30 min. It is known that the maximum floc size, d_{max}, scales with inverse square root of the global velocity gradient ($d_{max} \propto G^{-1/2}$), although to do this analysis would require subsequent studies run at different speeds, which was not the focus of this study.[27,46,61] For even more specific information on the local velocity gradients and stress distribution, a particle imaging velocimetry (PIV) setup would be needed. Because the global velocity gradient does not vary between experiments, the differences in floc size and floc growth rate are largely due to the interplay between increasing bentonite aggregate size and less expanded polyelectrolyte conformation from decreased persistence length as the solution ionic strength increases.

What is interesting to note is that there is no appreciable difference in the growth rates between the lower and higher molecular weight polyelectrolytes. This largely has to do with using TWV flow for all experiments, which implies that the intervortex mass transfer during

mixing does not significantly vary. Intervortex mass transfer can be quantified by an effective dispersion coefficient determined for this particular TC cell by Wilkinson and Dutcher,[38] which can be expressed as

$$D_z^* = 2\lambda k_{cb} \#(4)$$

where D_z^* is the effective dispersion coefficient in $m^2 \cdot s^{-1}$, λ is the axial wavelength of the vortex (~1 cm for vortices present here), and k_{cb} is the intermixing coefficient in $m\ s^{-1}$.[38,63] The values of D_z^* vary from 5.3 x 10^{-5} $m^2 \cdot s^{-1}$ at [I] = 0 mM and 1.3 mM, 6.7 x 10^{-5} $m^2 \cdot s^{-1}$ at [I] = 10 mM, and 6.2 x 10^{-5} $m^2 \cdot s^{-1}$ at [I] = 100 mM for 4190SH and from 5.6 x 10^{-5} $m^2 \cdot s^{-1}$ at [I] = 0 mM, 6.3 x 10^{-5} $m^2 \cdot s^{-1}$ at [I] = 1.3 mM, 6.2 x 10^{-5} $m^2 \cdot s^{-1}$ at [I] = 10 mM, and 5.9 x 10^{-5} $m^2 \cdot s^{-1}$ at [I] = 100 mM for 4190SSH for Stage 1 mixing. The trend is similar during Stage 2 mixing, where the values of D_z^* vary from 5.0 x 10^{-5} $m^2 \cdot s^{-1}$ at [I] = 0 mM to 5.8 x 10^{-5} $m^2 \cdot s^{-1}$ at [I] = 100 mM for 4190SH and from 5.2 x 10^{-5} $m^2 \cdot s^{-1}$ at [I] = 0 mM to 5.5 x 10^{-5} $m^2 \cdot s^{-1}$ at [I] = 100 mM for 4190SSH. The effective dispersion coefficient is highest at [I] = 10 mM and correlates with this case having the highest growth rate well, which indicates that the solution properties do indeed affect the trends described previously. There is a small delay in the floc growth curves for the 4190SH case at [I] = 0 mM and [I] = 1.3 mM compared to the 4190SSH by approximately 30 s and 100 s, respectively, which is due to the small increase in the effective dispersion coefficient for the 4190SSH case during Stage 1 mixing.

2.3 Ionic Strength and Molecular Weight Effects on Floc Morphology and Number

Another key parameter to examine in addition to floc size and floc growth rate is floc morphology as a function of ionic strength and polyelectrolyte molecular weight. Sedimentation and filtration of flocs for effective separation from water depend on the floc morphology and is related to both floc size and density.[27] Shear gradients present during the mixing process can

411 alter the floc structure with time, which can also have consequences for removal efficiency. Floc
412 morphology can be quantified using a non-dimensional parameter known as a fractal dimension.
413 To obtain a three-dimensional mass fractal dimension, light scattering techniques are typically
414 used, which requires the removal of sample flocs from their native environment.[58,64,65] One of the
415 major advantages of the TC cell used in this study is that the combination of the optically clear,
416 glass outer cylinder and the radial injection capabilities of the inner cylinder allows for
417 determination of the fractal dimension throughout the duration of the flocculation process via
418 image analysis without floc removal. The only difference between determining a fractal
419 dimension with image analysis and light scattering is that image analysis yields a two-
420 dimensional, rather than a three-dimensional, fractal dimension.[27,47,66]

421 The two-dimensional fractal dimension, D_{sf}, was obtained by linearly regressing the log
422 of the cross-sectional floc area against the log of the floc perimeter for each ten second data set.
423 The closer the D_{sf} value is to 1, the more circular in cross-section the floc is whereas the closer
424 D_{sf} is to 2, the less circular and more rod-like the cross-section of the floc is. Figure 5 shows the
425 evolution of D_{sf} with time during Stage 1 and Stage 2 mixing as a function of ionic strength and
426 polyelectrolyte molecular weight. The flocs are initially less circular (i.e. D_{sf} is closer to 2 than to
427 1) due to increased aggregate-aggregate collisions from orthokinetic aggregation, which is the
428 driving force behind flocculation.[7,59,66] The fractal dimension asymptotically decreases toward
429 unity in all cases, indicating that the floc morphology is more circular. This suggests that shear-
430 induced rounding dominates aggregate-aggregate collisions, particularly because a turbulent
431 flow type was used throughout the duration of the experiment, which echoes what was observed
432 in a prior study by Metaxas et al.[39] This shear rounding trend also correlates to results observed
433 from Spicer et al.[61] for the temporal evolution in the floc structure with varying the shear rates in

a baffled stir tank. In their study, they also observed a decrease in the 2-D fractal dimension until it asymptotes to a steady state value, indicating that there is preferential breakage of the flocs at weaker points (i.e. their edges) from subjecting the flocs for extended periods of time to shear forces present in the flow.

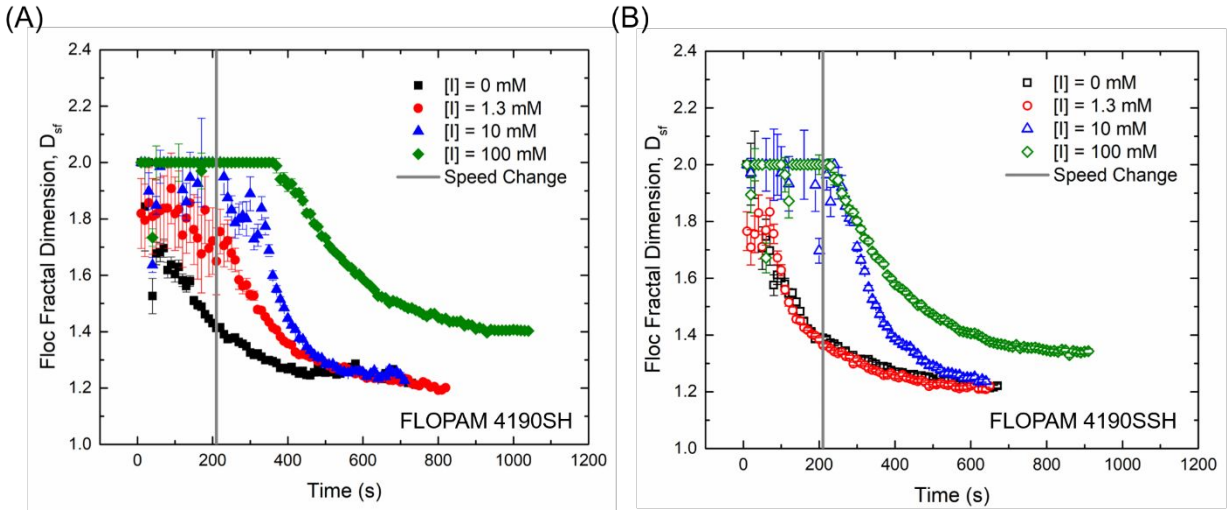

Figure 5: Floc morphology quantified as a 2-D perimeter-based fractal dimension, D_{sf}, as a function of ionic strength with time for the (A) lower molecular weight cationic polyacrylamide flocculant (4190SH) and the (B) higher molecular weight cationic polyacrylamide flocculant (4190SSH). The vertical gray line depicts where the inner cylinder speed transitions from Ω_i = 0.50 s^{-1} to Ω_i = 0.46 s^{-1}.

Another factor to consider here is how the individual bentonite sheets interact with each other prior to the addition of CPAM. It was previously mentioned that bentonite sheets adopt a porous, edge-face structure at lower ionic strengths. As the ionic strength increases, the bentonite sheets adopt a more edge-edge structure to ultimately, a denser, face-face packed structure.[16,17] Figure 5 and

show that the D_{sf} values increase with increasing ionic strength, indicating that the flocs are less circular in cross-section. At the end of the logistic growth fits, the D_{sf} values increased from 1.21 ± 0.01 at [I] = 0 mM to 1.4 ± 0.1 at [I] = 100 mM for 4190SH, and increased from

1.22 ± 0.06 at [I] = 0 mM to 1.4 ± 0.1 at [I] = 100 mM for 4190SSH. This implies that flocs at higher ionic strengths are more resistant to shear-induced rounding, which is most likely due to the denser nature of the bentonite aggregates at higher ionic strengths. Interestingly, these results contradict what Wilkinson et al.[21] found, where the flocs at [I] = 100 mM had smaller fractal dimensions than those at [I] = 10 mM. However, it should be noted that the fractal dimension for flocs at [I] = 0 mM or [I] = 1.3 mM were not measured in the Wilkinson study, and jar tests were used, where the flow field is not nearly as homogeneous as the TWV flow used in the present study.[34] Between the two polyelectrolytes used, there was a statistically insignificant difference between the fractal dimension values at injection, at the speed change, and at the end of the logistic growth fit. This result further suggests that the initial bentonite aggregate structure, which differs because of changes in the ionic strength of the solution, determines the fractal dimension trends.

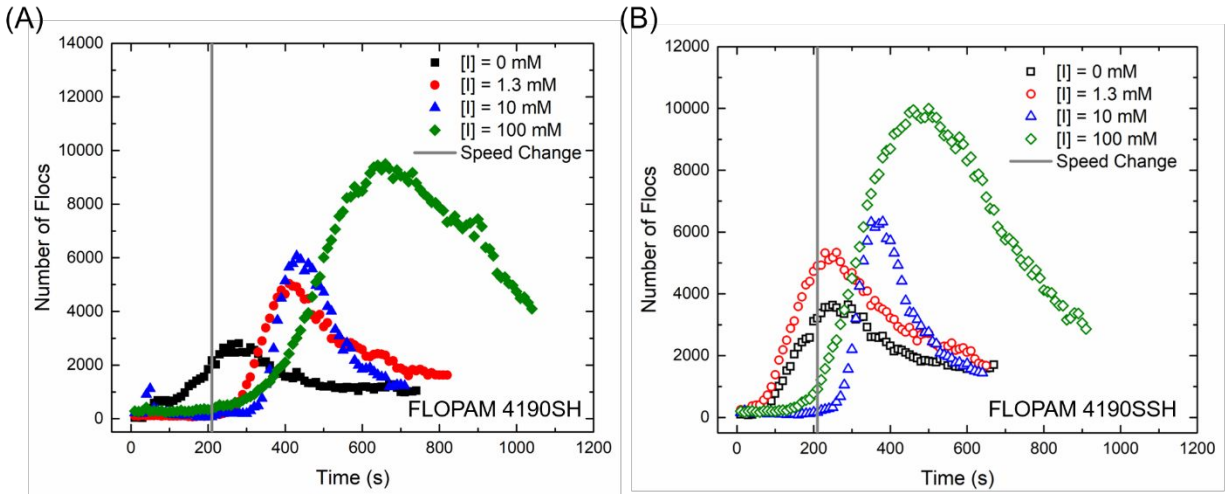

Figure 6: Number of flocs as a function of solution ionic strength with time for the (A) lower molecular weight cationic polyacrylamide flocculant (4190SH) and the (B) higher molecular weight cationic polyacrylamide flocculant (4190SSH). The vertical gray line depicts where the inner cylinder speed transitions from $\Omega_i = 0.50$ s^{-1} to $\Omega_i = 0.46$ s^{-1}.

In addition to differences in floc morphology as a function of ionic strength, the number of flocs present in the suspension differs with ionic strength. Because the persistence lengths of the polyelectrolytes are longer and therefore adopt a less expanded conformation in solution, and the initial bentonite aggregate sizes are lower at lower ionic strengths as compared to higher ionic strengths, more of the bentonite aggregates present in the suspension can be incorporated to form a floc. This is reflected in the larger floc sizes observed at lower ionic strengths in Figure 2, Figure 3, and Table 1. Larger floc sizes indicate less flocs in the suspension, which is what is observed in Figure 6. The maximum number of flocs increases from ~3000 flocs up to ~9000 flocs for 4190SH and from ~3500 flocs up to ~10,000 flocs for 4190SSH as ionic strength increases. The numbers are slightly higher for the 4190SSH as its longer length compared to 4190SH allows it to adsorb to more bentonite aggregates in the suspension.

Table 1: Summary of relevant parameters of the flocculation studies including the solution ionic strength, the polyelectrolyte concentration used with optimal dose or overdose indicated in parentheses, the maximum floc size, the floc growth rate, and the fractal dimension where the polyelectrolyte is injected (30 s), at the speed change from Stage 1 to Stage 2 mixing (210 s), and at the end of the region where growth plateaus (varies for each condition). The errors for the mean values represent 95% confidence intervals.

	Ionic Strength (mM)	Polyelectrolyte Concentration (ppm)	Max. Floc Size, R_g (mm)	Floc Growth Rate, r (mm·s^{-1})	D_{sf} at Injection	D_{sf} at Speed Change	D_{sf} at End of Fit
FLOPAM 4190SH (MW = 4-6 x 10^6 g·mol^{-1})	0	8.0 (optimal dose)	1.8 ± 0.3	0.010 ± 0.002	1.8 ± 0.6	1.5 ± 0.1	1.21 ± 0.01
	1.3	11.9 (optimal dose)	1.5 ± 0.5	0.011 ± 0.001	1.8 ± 0.4	1.7 ± 0.2	1.24 ± 0.06
	10	4.0 (optimal dose)	1.5 ± 0.5	0.020 ± 0.003	2.0 ± 0.1	2.0 ± 0.0	1.25 ± 0.09
	100	1.0 (optimal dose)	0.4 ± 0.1	0.008 ± 0.005	1.9 ± 0.1	1.8 ± 0.2	1.4 ± 0.1
	100	8.0 (overdose)	0.7 ± 0.4	0.0101 ± 0.0001	2.0 ± 0.0	1.55 ± 0.06	1.36 ± 0.08

	Ionic Strength (mM)	Polyelectrolyte Concentration (ppm)	Max. Floc Size, R_g (mm)	Floc Growth Rate, r (mm·s^{-1})	D_{sf} at Injection	D_{sf} at Speed Change	D_{sf} at End of Fit
FLOPAM 4190SSH (MW = 8-11 x 10^6 g·mol^{-1})	0	7.0 (optimal dose)	1.9 ± 0.2	0.008 ± 0.004	2.0 ± 0.2	1.41 ± 0.04	1.22 ± 0.06
	1.3	7.0 (optimal dose)	1.7 ± 0.6	0.012 ± 0.001	1.9 ± 0.3	1.4 ± 0.1	1.3 ± 0.1
	10	5.0 (optimal dose)	1.6 ± 0.1	0.020 ± 0.002	2.0 ± 0.0	2.0 ± 0.0	1.22 ± 0.03
	100	1.5 (optimal dose)	0.6 ± 0.3	0.009 ± 0.005	1.9 ± 0.3	1.8 ± 0.3	1.4 ± 0.1
	100	7.0 (overdose)	0.9 ± 0.8	0.010 ± 0.005	2.0 ± 0.0	1.7 ± 0.3	1.33 ± 0.07

2.4 Effects of Optimal Dosing and Overdosing on Floc Growth

To further illustrate the effects of overdosing a suspension with polyelectrolyte flocculant, an experiment was conducted to compare the floc size and floc growth rates between the optimal dose required for [I] = 100 mM as determined from Figure 1 for both polyelectrolytes used in this study. Figure 7(A) shows the floc size for the optimal dose cases (green symbols) with the corresponding overdose cases (purple symbols) for the lower molecular weight CPAM (closed diamonds) and the higher molecular weight CPAM (open triangles). The concentrations for the overdose case are 8.0 ppm for 4190SH and 7.0 ppm for 4190SSH, which are the concentrations used for the [I] = 0 mM case as shown in Table 1. There is no statistical difference in the maximum floc size and the floc growth rate between the optimal and overdose cases for both polyelectrolytes according to Table 1. To make it more apparent that there is no appreciable difference between the optimal and overdose cases, the floc size normalized by the maximum floc size was plotted against the adjusted time (where all growth starts at 0 s) in Figure 7(B). Using a higher concentration polyelectrolyte does not result in an increased flocculation performance compared to the smaller, optimal dose. Using more of the polyelectrolyte could potentially result in restabilization of the particulate as described earlier.[1] At an industrial scale,

using more flocculant than needed can be cost-prohibitive as more polyelectrolyte would be used and any excess polyelectrolyte would have to be filtered downstream prior to discharging the water.[48]

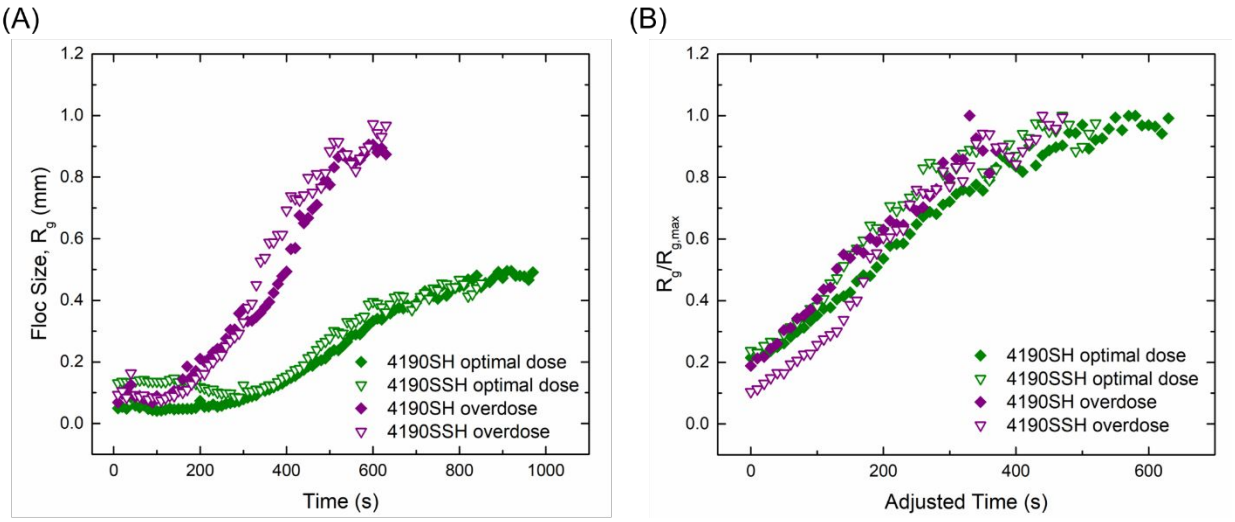

Figure 7: (A) Comparison of optimal dose (green symbols) and overdose (purple symbols) floc growth with time using the lower (4190SH, solid diamonds) and higher (4190SSH, open triangles) molecular weight polyelectrolyte flocculants at [I] = 100 mM. To better compare the floc growth of the optimal dose to overdose conditions, (B) shows the time adjusted such that all growth curves start at 0 s and the floc sizes normalized by the maximum floc size ($R_g/R_{g,max}$). There is no statistical difference in floc size or growth rate between optimal dose and overdose conditions for both flocculants studied.

3 Conclusion

The unique ability to non-intrusively inject one fluid into another fluid while harnessing the precise mixing capabilities of a TC cell offers unprecedented access to the entire flocculation process without having to remove flocs for further analysis. In this study, the ionic strength was varied in a bentonite suspension and two different molecular weights of polyelectrolyte flocculant were used at the same turbulent wavy vortex flow state generated by the TC cell to obtain the floc size, floc growth rate, 2-D floc fractal dimension (D_{sf}), and floc numbers with time. As the ionic strength increased, the floc size generally decreased while the floc growth rate

initially increased then decreased. This was due to charge screening effects, where the initial bentonite aggregate size increases but the polyelectrolyte persistence length decreases and its conformation is less expanded, hindering its ability to adsorb to and bridge multiple bentonite aggregates. The D_{sf} values increased (became less circular in cross-section) with ionic strength due to densification of bentonite aggregates because of charge screening, rendering the flocs more resistant to shear-induced breakage. An increase in ionic strength resulted in an increased in the number of flocs due to the inability of the polyelectrolytes to effectively bridge multiple bentonite aggregates as their respective persistence lengths decrease with increasing ionic strength, resulting in a less expanded conformation in solution. There were no appreciable differences with respect to maximum floc size, growth rate, and floc structure between the two molecular weights of CPAM tested in this study, with the exceptions of smaller optimal doses and slightly higher effective dispersion coefficients for the larger molecular weight polyelectrolyte. In summary, the solution ionic strength is a critical process variable to consider in a flocculation process as it can have ramifications for the solution behavior of both the particulate system and the flocculant.

Flocculation is a highly dynamic process, with results that depend on both the physicochemical properties of the solution, as well as the hydrodynamic properties of the mixing environment. With respect to the myriad of factors affecting polyelectrolyte-mediated flocculation, this study only begins to scratch the surface. Here, only one turbulent vortex type (TWV) was used to study the flocculation of bentonite with cationic polyacrylamide as a function of ionic strength and polymer molecular weight. It would be of interest to study how the results presented here compare with a different turbulent flow state or with a laminar flow state, such as laminar wavy vortex flow. Fundamental understanding of the effect of solution

properties and flow parameters can potentially be used to optimize processes that utilized polymer-driven flocculation of a solid particulate, such as water treatment operations.

4 Conflicts of Interest

There are no conflicts to declare.

5 Acknowledgments

This work was partially supported by the National Science Foundation through the University of Minnesota MRSEC under Award Numbers DMR-1420013 and DMR-2011401. Part of this work was carried out in the College of Science and Engineering Polymer Characterization Facility, University of Minnesota, which has received capital equipment funding from the NSF through the UMN MRSEC program under Award Number DMR-1420013. Acknowledgment is made to the donors of the American Chemical Society Petroleum Research Fund for partial support of this research. A.M. was supported through a National Science Foundation Graduate Research Fellowship. R.O. was supported by a Research Experience for Undergraduates fellowship through the UMN MRSEC. The authors would like to thank Lisa Zeeb for designing the graphical abstract.

6 References

1 B. Bolto and J. Gregory, Organic polyelectrolytes in water treatment, *Water Res.*, 2007, **41**, 2301–2324.

2 S. M. R. Shaikh, M. S. Nasser, I. Hussein, A. Benamor, S. A. Onaizi and H. Qiblawey, Influence of polyelectrolytes and other polymer complexes on the flocculation and rheological behaviors of clay minerals: A comprehensive review, *Sep. Purif. Technol.*, 2017, **187**, 137–161.

3 L. Feng, M. C. Stuart and Y. Adachi, Dynamics of polyelectrolyte adsorption and colloidal flocculation upon mixing studied using mono-dispersed polystyrene latex particles, *Adv. Colloid Interface Sci.*, 2015, **226**, 101–114.

4 D. Bonn, Y. Amarouchène, C. Wagner, S. Douady and O. Cadot, Turbulent drag reduction by polymers, *J. Phys. Condens. Matter*, 2005, **17**, S1195–S1202.

5 M. S. Nasser and A. E. James, Effect of polyacrylamide polymers on floc size and rheological behaviour of kaolinite suspensions, *Colloids Surfaces A Physicochem. Eng. Asp.*, 2007, **301**, 311–322.

6 B. Oyegbile, P. Ay and S. Narra, Introduction Flocculation kinetics and hydrodynamic interactions in natural and engineered flow systems: A review, *Environ. Eng. Res*, 2016, **21**, 1–14.

7 J. C. Berg, *An Introduction to Interfaces and Colloids*, World Scientific, 2009.

8 Z. Zhu, H. Wang, J. Yu and J. Dou, On the Kaolinite Floc Size at the Steady State of Flocculation in a Turbulent Flow, *PLoS One*, 2016, **11**, e0148895.

9 J. Roussy, M. Van Vooren, B. A. Dempsey and E. Guibal, Influence of chitosan characteristics on the coagulation and the flocculation of bentonite suspensions, *Water Res.*, 2005, **39**, 3247–3258.

10 N. Levy, S. Magdassi and Y. Bar-Or, Physico-chemical aspects in flocculation of bentonite suspensions by a cyanobacterial bioflocculant, *Water Res.*, 1992, **26**, 249–254.

11 S. M. Shaikh, M. Nasser, I. A. Hussein and A. Benamor, Investigation of the effect of polyelectrolyte structure and type on the electrokinetics and flocculation behavior of bentonite dispersions, *Chem. Eng. J.*, 2017, **311**, 265–276.

12 G. Waajen, F. Van Oosterhout, G. Douglas and M. Lürling, Management of eutrophication in Lake De Kuil (The Netherlands) using combined flocculant-Lanthanum modified bentonite treatment, *Water Res.*, 2016, **97**, 83–95.

13 J. D. G. Durán, M. M. Ramos-Tejada, F. J. Arroyo and F. González-Caballero, Rheological and Electrokinetic Properties of Sodium Montmorillonite Suspensions, *J. Colloid Interface Sci.*, 2000, **229**, 107–117.

14 A. Cadene, S. Durand-Vidal, P. Turq and J. Brendle, Study of individual Na-montmorillonite particles size, morphology, and apparent charge, *J. Colloid Interface Sci.*, 2005, **285**, 719–730.

15 D. Heath and T. . Tadros, Influence of pH, electrolyte, and poly(vinyl alcohol) addition on the rheological characteristics of aqueous dispersions of sodium montmorillonite, *J. Colloid Interface Sci.*, 1983, **93**, 307–319.

16 J. S. Chen, Rheological Behavior of Na-Montmorillonite Suspensions at Low Electrolyte Concentration, *Clays Clay Miner.*, 1990, **38**, 57–62.

17 J. Stawiński, Influence of Calcium and Sodium Concentration on the Microstructure of Bentonite and Kaolin, *Clays Clay Miner.*, 1990, **38**, 617–622.

18 M. S. Zbik, R. S. C. Smart and G. E. Morris, Kaolinite flocculation structure, *J. Colloid Interface Sci.*, 2008, **328**, 73–80.

19 M. S. Żbik, D. J. Williams, Y.-F. Song and C.-C. Wang, The formation of a structural framework in gelled Wyoming bentonite: direct observation in aqueous solutions., *J. Colloid Interface Sci.*, 2014, **435**, 119–27.

20 N. Wilkinson, A. Metaxas, E. Ruud, E. Raethke, S. Wickramaratne, T. M. Reineke and C. S. Dutcher, Internal structure visualization of polymer - clay flocculants using fluorescence, *Colloids Interface Sci. Commun.*, 2016, **10–11**, 1–5.

21 N. Wilkinson, A. Metaxas, E. Brichetto, S. Wickramaratne, T. M. Reineke and C. S. Dutcher, Ionic strength dependence of aggregate size and morphology on polymer-clay flocculation, *Colloids Surfaces A Physicochem. Eng. Asp.*, 2017, **529**, 1037–1046.

22 N. Wilkinson, A. Metaxas, C. Quinney, S. Wickramaratne, T. M. Reineke and C. S. Dutcher, pH dependence of bentonite aggregate size and morphology on polymer-clay flocculation, *Colloids Surfaces A Physicochem. Eng. Asp.*, 2018, **537**, 281–286.

23 N. Mayordomo, C. Degueldre, U. Alonso and T. Missana, Size distribution of FEBEX bentonite colloids upon fast disaggregation in low-ionic strength water, *Clay Miner.*, 2016, **51**, 213–222.

24 X. Yan and X. Zhang, Interactive effects of clay and polyacrylamide properties on flocculation of pure and subsoil clays, *Soil Res.*, 2014, **52**, 727.

25 C. Walldal and B. Åkerman, Effect of Ionic Strength on the Dynamic Mobility of Polyelectrolytes, *Langmuir*, 1999, **15**, 5237–5243.

26 R. H. Colby, Structure and linear viscoelasticity of flexible polymer solutions: comparison of polyelectrolyte and neutral polymer solutions, *Rheol Acta*, 2010, **49**, 425–442.

27 P. T. Spicer, W. Keller and S. E. Pratsinis, The Effect of Impeller Type on Floc Size and Structure during Shear-Induced Flocculation, *J. Colloid Interface Sci.*, 1996, **184**, 112–122.

28 M. Soos, L. Ehrl, M. U. Bäbler and M. Morbidelli, Aggregate breakup in a contracting nozzle., *Langmuir*, 2010, **26**, 10–8.

29 C. D. Andereck, S. S. Liu and H. L. Swinney, Flow regimes in a circular Couette system with independently rotating cylinders, *J. Fluid Mech.*, 2006, **164**, 155.

30 C. S. Dutcher and S. J. Muller, Explicit analytic formulas for Newtonian Taylor-Couette

primary instabilities., *Phys. Rev. E. Stat. Nonlin. Soft Matter Phys.*, 2007, **75**, 047301.

31 C. S. Dutcher and S. J. Muller, Spatio-temporal mode dynamics and higher order transitions in high aspect ratio Newtonian Taylor–Couette flows, *J. Fluid Mech.*, 2009, **641**, 85.

32 M. A. Fardin, C. Perge and N. Taberlet, "The hydrogen atom of fluid dynamics" – introduction to the Taylor–Couette flow for soft matter scientists, *Soft Matter*, 2014, **10**, 3523.

33 M. V. Majji, S. Banerjee and J. F. Morris, Inertial flow transitions of a suspension in Taylor–Couette geometry, *J. Fluid Mech.*, 2018, **835**, 936–969.

34 C. Coufort, D. Bouyer and A. Liné, Flocculation related to local hydrodynamics in a Taylor–Couette reactor and in a jar, *Chem. Eng. Sci.*, 2005, **60**, 2179–2192.

35 C. Selomulya, G. Bushell, R. Amal and T. D. Waite, Aggregate properties in relation to aggregation conditions under various applied shear environments, *Int. J. Miner. Process.*, 2004, **73**, 295–307.

36 L. Guérin, C. Coufort-Saudejaud, A. Liné and C. Frances, Dynamics of aggregate size and shape properties under sequenced flocculation in a turbulent Taylor-Couette reactor, *J. Colloid Interface Sci.*, 2017, **491**, 167–178.

37 N. Wilkinson and C. S. Dutcher, Taylor-Couette flow with radial fluid injection, *Rev. Sci. Instrum.*, 2017, **88**, 083904.

38 N. A. Wilkinson and C. S. Dutcher, Axial mixing and vortex stability to in situ radial injection in Taylor-Couette laminar and turbulent flows, *J. Fluid Mech.*, 2018, **854**, 324–347.

39 A. Metaxas, N. Wilkinson, E. Raethke and C. S. Dutcher, In situ polymer flocculation and growth in Taylor-Couette flows, *Soft Matter*, 2018, **14**, 8627–8635.

40 Y. Adachi and T. Wada, Initial Stage Dynamics of Bridging Flocculation of Polystyrene Latex Spheres with Polyethylene Oxide, *J. Colloid Interface Sci.*, 2000, **229**, 148–154.

41 Y. Adachi and J. Xiao, Initial stage of bridging flocculation of PSL particles induced by an addition of polyelectrolyte under high ionic strength, *Colloids Surfaces A Physicochem. Eng. Asp.*, 2013, **435**, 127–131.

42 S. Kaufhold, R. Dohrmann, D. Koch and G. Houben, The pH of Aqueous Bentonite Suspensions, *Clays Clay Miner.*, 2008, **56**, 338–343.

43 S. D. T. Axford and T. M. Herrington, Determination of aggregate structures by combined light-scattering and rheological studies, *J. Chem. Soc. Faraday Trans.*, 1994, **90**, 2085.

44 G. C. Bushell, Y. D. Yan, D. Woodfield, J. Raper and R. Amal, On techniques for the measurement of the mass fractal dimension of aggregates, *Adv. Colloid Interface Sci.*, 2002, **95**, 1–50.

45 J. A. Rice, E. Tombácz and K. Malekani, Applications of light and X-ray scattering to characterize the fractal properties of soil organic matter, *Geoderma*, 1999, **88**, 251–264.

46 D. Bouyer, C. Coufort, A. Liné and Z. Do-Quang, Experimental analysis of floc size distributions in a 1-L jar under different hydrodynamics and physicochemical conditions, *J. Colloid Interface Sci.*, 2005, **292**, 413–428.

47 M. Vlieghe, C. Coufort-Saudejaud, C. Frances and A. Liné, *In situ* characterization of floc morphology by image analysis in a turbulent Taylor-Couette reactor, *AIChE J.*, 2014, **60**, 2389–2403.

48 C. S. Lee, J. Robinson and M. F. Chong, A review on application of flocculants in wastewater treatment, *Process Saf. Environ. Prot.*, 2014, **92**, 489–508.

49 A. Blanco, C. Negro, E. Fuente and J. Tijero, Effect of Shearing Forces and Flocculant Overdose on Filler Flocculation Mechanisms and Floc Properties, *Ind. Eng. Chem. Res.*, 2005, **44**, 9105–9112.

50 A. Daryabeigi Zand and H. Hoveidi, *Comparing Aluminium Sulfate and Poly-Aluminium Chloride (PAC) Performance in Turbidity Removal from Synthetic Water*, 2015, vol. 2.

51 Y. Sakhawoth, L. J. Michot, P. Levitz and N. Malikova, Flocculation of Clay Colloids Induced by Model Polyelectrolytes: Effects of Relative Charge Density and Size, *ChemPhysChem*, 2017, **18**, 2756–2765.

52 M. A. Yukselen and J. Gregory, The effect of rapid mixing on the break-up and re-formation of flocs, *J. Chem. Technol. Biotechnol.*, 2004, **79**, 782–788.

53 E. Barbot, P. Dussouillez, J. Y. Bottero and P. Moulin, Coagulation of bentonite suspension by polyelectrolytes or ferric chloride: Floc breakage and reformation, *Chem. Eng. J.*, 2010, **156**, 83–91.

54 Y. V. Bukhman, N. W. DiPiazza, J. Piotrowski, J. Shao, A. G. W. Halstead, M. D. Bui, E. Xie and T. K. Sato, Modeling Microbial Growth Curves with GCAT, *BioEnergy Res.*, 2015, **8**, 1022–1030.

55 D. Mikeš, A Simple Floc-Growth Function for Natural Flocs in Estuaries, *Math Geosci*, 2011, **43**, 593–606.

56 N. Deepnarain, S. Kumari, J. Ramjith, F. M. Swalaha, V. Tandoi, K. Pillay and F. Bux, A logistic model for the remediation of filamentous bulking in a biological nutrient removal wastewater treatment plant, *Water Sci. Technol.*, 2015, **72**, 391–405.

57 G. Durand, F. Lafuma and R. Audebert, in *Trends in Colloid and Interface Science II*, Steinkopff, Darmstadt, 1988, pp. 278–282.

58 Peter Jarvis, A. Bruce Jefferson and S. A. Parsons, Breakage, Regrowth, and Fractal Nature of Natural Organic Matter Flocs, *Environ. Sci. Technol.*, 2005, **39**, 2307–2314.

59 W. Yu, J. Gregory, L. Campos and G. Li, The role of mixing conditions on floc growth, breakage and re-growth, *Chem. Eng. J.*, 2011, **171**, 425–430.

60 L. Guibai and J. Gregory, Flocculation and sedimentation of high-turbidity waters, *Water Res.*, 1991, **25**, 1137–1143.

61 P. T. Spicer and S. E. Pratsinis, Shear-induced flocculation: The evolution of floc structure

and the shape of the size distribution at steady state, *Water Res.*, 1996, **30**, 1049–1056.

62 D. Bouyer, A. Liné and Z. Do-Quang, Experimental analysis of floc size distribution under different hydrodynamics in a mixing tank, *AIChE J.*, 2004, **50**, 2064–2081.

63 N. Ohmura, K. Kataoka, Y. Shibata and T. Makino, Effective mass diffusion over cell boundaries in a Taylor-Couette flow system, *Chem. Eng. Sci.*, 1997, **52**, 1757–1765.

64 T. Li, Z. Zhu, D. Wang, C. Yao and H. Tang, Characterization of floc size, strength and structure under various coagulation mechanisms, *Powder Technol.*, 2006, **168**, 104–110.

65 T. Li, Z. Zhu, D. Wang, C. Yao and H. Tang, The strength and fractal dimension characteristics of alum–kaolin flocs, *Int. J. Miner. Process.*, 2007, **82**, 23–29.

66 Z. Zhu, J. Yu, H. Wang, J. Dou and C. Wang, Fractal Dimension of Cohesive Sediment Flocs at Steady State under Seven Shear Flow Conditions, *Water*, 2015, **7**, 4385–4408.

Graphical Abstract

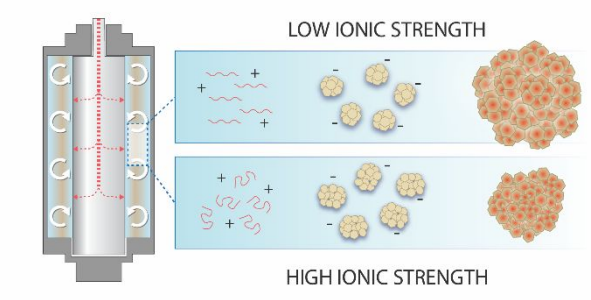

Graphical abstract summary: Increased charge screening from increased ionic strength of a bentonite-laden suspension for flocculation in a Taylor-Couette cell capable of radial injection results in an interplay between increased bentonite aggregate size and decreased ability for the polyelectrolyte to bridge multiple aggregates due to decreasing persistence length, resulting in a less expanded polymer conformation in solution.